The Southern Ocean sea surface temperature response to ozone depletion: A multi-model comparison

W. J. M. Seviour[1,2], F. Codron[3], E. W. Doddridge[4], D. Ferreira[5], A. Gnanadesikan[1], M. Kelley[6], Y. Kostov[7], J. Marshall[4], L. M. Polvani[8], J. L. Thomas[1], D. W. Waugh[1,9]

1. *Department of Earth and Planetary Sciences, Johns Hopkins University, Baltimore MD, USA*
2. *School of Geographical Sciences, University of Bristol, Bristol, UK*
3. *LOCEAN/IPSL, Sorbonne Université, CNRS, IRD, MNHN, Paris, France*
4. *Department of Earth, Atmospheric, and Planetary Sciences, Massachusetts Institute of Technology, Cambridge MA, USA*
5. *Department of Meteorology, University of Reading, Reading, UK*
6. *NASA Goddard Institute for Space Studies, New York NY, USA*
7. *Department of Physics, University of Oxford, UK*
8. *Applied Physics and Applied Mathematics Department, and Department of Earth and Environmental Science, Lamont-Doherty Earth Observatory, Columbia University, New York NY, USA*
9. *School of Mathematics, University of New South Wales, Sydney, Australia*

May 2018

Submitted to *Journal of Climate*

Corresponding author: William J. M. Seviour, School of Geographical Sciences, University of Bristol, University Road, Bristol BS8 1SS, United Kingdom. Email: w.seviour@bristol.ac.uk

Abstract

The effect of the Antarctic ozone hole extends downwards from the stratosphere, with clear signatures in surface weather patterns including a positive trend in the Southern Annular Mode (SAM). Several recent studies have used coupled climate models to investigate the impact of these changes on Southern Ocean sea surface temperature (SST), notably motivated by the observed cooling from the late 1970s. Here we examine the robustness of these model results through comparison of both previously published and new simulations. We focus on the calculation of 'climate response functions' (CRFs), transient responses to an instantaneous step-change in ozone concentrations. The CRF for most models consists of a rapid cooling of SST, followed by a slower warming trend. However, inter-model comparison reveals large uncertainties, such that even the sign of the impact of ozone depletion on historical SST, when reconstructed from the CRF, remains unconstrained. Comparison of these CRFs with SST responses to a hypothetical step-change in the SAM, inferred through lagged linear regression, shows broadly similar results. Causes of uncertainty are explored by examining relationships between model climatologies and their CRFs. The inter-model spread in CRFs can be reproduced by varying a single subgrid-scale mixing parameter within a single model. Antarctic sea-ice CRFs are also calculated: these do not generally exhibit the two-time-scale behavior of SST, suggesting a complex relationship between the two. Finally, by constraining model climatology-response relationships with observational values, we conclude that ozone depletion in unlikely to have been the primary driver of the observed SST cooling trend.

1. Introduction

In contrast to the rapidly warming Arctic, sea surface temperature (SST) averaged over the Southern Ocean (SO) has exhibited a multidecadal cooling trend from the beginning of the satellite record in 1979 (Fan et al. 2014; Armour and Bitz 2016) (although this trend may have reversed since late-2016 [Meehl et al. 2019]). During the same period, there have also been significant changes in the Southern Hemisphere (SH) atmospheric circulation, including a poleward shift and intensification of the SH midlatitude jet, consistent with a positive trend in the Southern Annular Mode (SAM) (Swart and Fyfe 2012; Hande et al. 2012, Jones et al. 2016). There is mounting evidence that these atmospheric trends are significantly driven by stratospheric ozone depletion (Thompson et al. 2011), the influence of which extends downwards through the troposphere to the surface. Indeed, the impact of ozone depletion on the SH summertime atmospheric circulation has been shown to dominate that of rising greenhouse gas concentrations over the last several decades (Polvani et al. 2011; Gerber and Son 2014), although there remains significant uncertainty as to the contribution of natural variability (Thomas et al. 2015). However, it is an open question whether the cooling trend in SO SST is caused by these atmospheric circulation changes (and, in turn, may be linked to ozone depletion), whether it caused by other processes, or is simply a result of natural internal climate variability. Answering this question will be crucial to predict the future of SO temperatures as the ozone hole heals during coming decades.

A number of studies have used coupled climate models to investigate the impact of ozone depletion-driven atmospheric circulation trends on the SO. These have either compared annually-repeating “ozone hole” and control (pre-ozone depletion) simulations (Sigmond and Fyfe 2010;

71 Bitz and Polvani 2012), or used simulations with time-varying historical or predicted future ozone
72 concentrations (Smith et al. 2012; Sigmond and Fyfe 2014; Solomon et al. 2015). All such studies
73 have found that ozone depletion leads to a surface warming (see review by Previdi and Polvani
74 2014), concluding that ozone depletion has acted to oppose the observed cooling trend, rather than
75 driving it. These findings were surprising given that, on interannual time scales, a positive phase
76 of the SAM is known to induce a surface cooling poleward of 50°S; a response which is understood
77 to be predominantly forced by increased equatorward Ekman transport of cold waters near
78 Antarctica (Hall and Visbeck 2002, Ciasto and Thompson 2008). Motivated by this interannual
79 SAM-SST relationship, Goosse et al. (2009) proposed that the ozone-driven positive SAM trend
80 may indeed be responsible for the observed SST cooling, a conclusion which opposes the findings
81 from coupled climate models.
82
83 Recent advances have been made towards reconciling these seemingly contradictory results. In
84 particular, studies have focused on the time-dependence of the SST response to ozone depletion
85 through the calculation of 'climate response functions' (CRFs); the transient response to an
86 instantaneous step-change in ozone concentrations (Marshall et al. 2014). By using this idealized
87 ozone forcing, CRFs can reveal more clearly the time scales and mechanisms of the response than
88 simulations with more realistic transient ozone changes. Ferreira et al. (2015) calculated CRFs in
89 two coupled models: CCSM3.5 and an idealized coupled MITgcm configuration. They showed
90 that on shorter time scales (months to years), the ozone depletion CRF is characterized by SO SST
91 cooling, consistent with the SAM-SST interannual relationship. On longer time scales (years to
92 decades) this cooling is replaced by a warming associated with Ekman upwelling of warm water
93 from depth. Seviour et al. (2016) showed that this two-time-scale CRF also exists in the GFDL

ESM2Mc model, which has much greater variability associated with deep convection in the Weddell Sea (Cabré et al., 2017). However, there are large differences between the CRFs of these three models. For instance, the initial cooling period lasts about 20 years in MITgcm, 25 years in GFDL ESM2Mc, but just 5 years in CCSM3.5. The length of this cooling period may have a profound effect on our understanding of the influence of ozone depletion on historical SST. However, given that CRFs had been calculated in just three models (and one of these, MITgcm, used a highly-idealized configuration), it is not clear how robust this value is.

An alternative method to estimate the CRF, using lagged linear regression between the SAM and SST, was put forward by Kostov et al. (2017). Unlike the step-response simulations described above, this method makes use of pre-existing control simulations. While Kostov et al. (2017) found a two-time-scale CRF to exist in many of the models included in the Coupled Model Intercomparison Project phase 5 (CMIP5), they again noted large inter-model differences. They related differences in models' short- and long-term SST responses to their climatological Southern Ocean meridional SST gradient and vertical temperature inversion, respectively. These relationships are physically plausible if, as proposed by Ferreira et al. (2015), the short-term response is largely driven by meridional Ekman transport, and the long-term response by anomalous upwelling of warm subsurface water. However, the climatology-response relationships shown by Kostov et al. (2017) explained only about 50% and 20% of the inter-model variance of the short- and long-term responses respectively, indicating that several other factors may also play an important role. Indeed, Doddridge et al. (2019) proposed that the wind-driven upwelling is opposed by an eddy-driven circulation (a process known as eddy compensation), thereby limiting the ability of this upwelling to drive the long-term SST warming. The short-term SST cooling

response may also be significantly affected by increased low cloud cover associated with a positive SAM, as well as by surface freshening leading to a reduction in vertical mixing (Ferreira et al. 2015; Seviour et al 2017), both of which may add to inter-model variance in responses.

Here we provide a synthesis of the recent ozone depletion CRF studies described above, alongside new ensembles of CRF simulations using three additional coupled climate models. This allows us to identify the robust aspects of the simulated SST response to ozone depletion, as well as to determine inter-model differences. We also discuss these CRFs in the context of projected SST changes under realistic time-varying ozone concentrations. We go on to compare these fully-nonlinear ozone depletion CRF simulations with SAM-SST CRFs calculated from the same models using the lagged linear regression method of Kostov et al. (2017). Note that a direct comparison between these two approaches was not previously possible because ozone depletion CRF simulations have not been performed using any of the CMIP5 models considered by Kostov et al. (2017). In order to examine the sensitivity of models' CRFs to their climatology we vary the subgrid-scale eddy advection, which controls the strength of the climatological temperature inversion, in a single model. In doing so, we are able to isolate the role of the temperature inversion in determining the CRF, while keeping other factors (such as cloud-circulation feedbacks) fixed. Finally we discuss the relationship between models' SST and Antarctic sea ice responses.

Our paper is organized as follows: The next section describes the model simulations used, as well as the two approaches for estimating CRFs. Section 3a gives a comparison of fully-nonlinear ozone depletion CRFs, section 3b compares these with linear SAM-SST CRFs, and section 3c focuses

on the relationship between model climatologies and their CRFs. Section 4 discusses the results in the context of observed SO trends, and conclusions are presented in section 5.

2. Models and methodology

a. Models and ozone depletion climate response function (CRF) simulations

Ozone depletion CRFs are calculated using coupled climate model simulations in which the annual cycle of ozone concentrations is abruptly changed from pre-ozone depletion levels to contemporary "ozone hole" levels. All other forcings are kept constant at preindustrial levels. In order to separate the forced response to ozone depletion from internal climate variability, an ensemble of simulations with varying initial conditions is performed. The six ensembles of CRF simulations compared here are detailed in Table 1. For full descriptions of the previously published simulations the reader is directed to the appropriate references. It is noteworthy that, unlike other models, the MITgcm simulations used a highly idealized "double Drake" configuration (consisting of an aquaplanet with two 'sticks' of land extending from the North Pole to 35°S, separated by 90° longitude). The MITgcm simulations' ocean mixed layer also lacks a parameterization of vertical mixing, while the atmosphere does not have an explicit representation of ozone and just a single layer representing the stratosphere; the ozone perturbation is performed by introducing a seasonal reduction of shortwave absorption in this layer.

The CRF simulations with the Institut Pierre Simon Laplace (IPSL) CM5A-MR, have not been previously published. IPSL CM5A-MR is the mid-resolution version of the IPSL-CM5A model

(Dufresne et al. 2013), and has an atmospheric resolution of 1.25° with 39 vertical levels (including a resolved stratosphere), and an ocean resolution of 2° with 21 levels. A 24-member ensemble of 25-year CRF simulations was performed, all initialized from the long (300-year) equilibrated CMIP5 pre-industrial control simulation. The starting dates were taken at least 5-years apart, and chosen to ensure that (1) there was no large ensemble-mean trend in the Southern Ocean SST and sea-ice in the corresponding control 25-year periods, and (2) there was no spurious sampling of multi-decadal variability in the Atlantic (AMO) or Pacific (IPO). For each ensemble member, the prescribed seasonal cycle of ozone concentration was changed on January 1st of the starting year from pre-industrial to that of year 2000 used in the CMIP5 historical simulations.

We also present an ensemble of CRF simulations using the GFDL ESM2Mc model as in Seviour et al. (2016), but with a perturbation to the model's subgrid-scale eddy parameterization. The purpose of this ensemble is to study the effect of changing the climatological ocean state while keeping the atmospheric response approximately fixed. Specifically, we increase the minimum value of the diffusion coefficient, A_{GM}, in the Gent-McWilliams eddy advection scheme (Gent and McWilliams 1990) from 200 m^2s^{-1} to 600 m^2s^{-1} (hereafter these experiments are labelled GM200 and GM600). Under this parameterization scheme A_{GM} varies spatially depending upon the meridional gradient of vertical shear between 100-2000 m, with a minimum and maximum value imposed (fixed at 1400 m^2s^{-1}). Because the resulting overturning scales as the product of the isopycnal slope and the buoyancy frequency, changing the minimum value has a large impact in the weakly stratified Southern Ocean, but very little effect across much of the rest of the global ocean (Thomas et al. 2018).

185 *b. SAM climate response functions*

186

187 An alternative method for estimating CRFs, using models' internal climate variability, was put
188 forward by Kostov et al. (2017), and is briefly described here. The evolution of SO SST in a control
189 simulation, $SST_{cntrl}(t)$, can be expressed as a convolution of the SAM forcing with a quasi-Green's
190 function *G(t)*,

191

192 $$\mathrm{SST}_{\mathrm{cntrl}}(t) = \int_0^{+\infty} G(t')\mathrm{SAM}_{\mathrm{cntrl}}(t-t')dt' + \varepsilon \quad (1)$$

193 $$\approx \int_0^{t_{\max}} G(t')\mathrm{SAM}_{\mathrm{cntrl}}(t-t')dt' + \varepsilon \quad (2)$$

194

195 where $SAM_{cntrl}(t)$ is the SAM index normalized by its standard deviation, t_{max} is an imposed
196 maximum cutoff lag, and ε is residual noise. Importantly, the underlying assumption of Eq. 1 is
197 that the ocean response to SAM forcing is linear, such that there is not a significant feedback
198 between the SAM and SO SST, at least on the relevant time scales of years to decades. Equation
199 (2) can be discretized to give

200

201 $$\mathrm{SST}_{\mathrm{cntrl}}(t) = \sum_{i=0}^{I} G(t_i')\,\mathrm{SAM}_{\mathrm{cntrl}}(t-t')\Delta t' + \varepsilon, \ \text{with} \ \ t_I' = t_{\max} \quad (3)$$

202

203 where each interval **Δ**t' is taken to be one year, and the coefficients $G(t_i')$ represent the response
204 at different time lags to a 1 standard deviation SAM impulse. Multiple linear least-squares
205 regression between the SST time series and lagged SAM time series is used to estimate each $G(t_i')$
206 for $i = 0, 1, \ldots I$. Integrating $G(t_i')$ in time then gives the SO SST step-response function (CRF)

207

$$\mathrm{CRF}_{\mathrm{SAM}}(t) = \sum_{i=0}^{I} G(t_i'), \text{ with } t_I' = t \quad (4)$$

Following Kostov et al. (2017), we vary the value of $t_{\max}$ (50, 75, 100, and 150 years) and select shorter subsets of the control simulation time series to obtain a range of fits. We also calculate the uncertainty in each least-squares fit. These uncertainties are combined in quadrature to obtain an overall uncertainty estimate in $\mathrm{CRF}_{\mathrm{SAM}}(t)$.

The impact of ozone depletion on the SAM is highly seasonal, with the largest surface impacts in the austral summer and autumn, lagging the seasonal cycle ozone forcing by approximately 3 months (e.g., Thompson and Solomon 2002, Polvani et al. 2011). Hence, in order to make the closest possible comparison with the ozone depletion CRF simulations, we set $\mathrm{SAM}_{\mathrm{cntrl}}(t)$ to represent the December-May averaged SAM index. We here define the SAM index as the difference between the zonally-averaged sea-level pressure at 40°S and 65°S, as in Swart et al (2015).

c. Inferring the response to time-dependent forcing

Although CRFs represent the response to an idealized instantaneous ozone hole, they can be related to changes under realistic time-varying ozone concentrations by linear convolution theory (Hasselmann et al. 1993; Kostov et al. 2018). Given a forcing function $F(t)$, and a CRF for the step response per unit forcing, then the time-dependent forced SST response is given by

$$SST(t) = \int_0^t CRF(t - t') \frac{\partial F}{\partial t}(t') dt' + \varepsilon \quad (5)$$

For the case of ozone depletion we take $F(t)$ to be the October-mean polar cap (60-90°S) averaged total column ozone in Dobson Units (DU); hence the dimensions of the CRF are [K DU^{-1}]. In practice, the lower bound of the integral in Eq. 2, t=0, is taken to be at some time when the forcing can be assumed negligible; here we take this to be the year 1955, before which stratospheric ozone changes are likely to have been very small (e.g. Cionni et al. 2011).

3. Results

a. Inter-model comparison of ozone climate response functions

The ensemble-mean responses of zonal-mean wind stress are broadly similar in all six ensembles of CRF simulations, consisting of a decline in wind stress equatorward of the climatological maximum and a wind stress increase poleward of the maximum (Fig. 1). These wind stress responses occur rapidly within the first year of the ozone perturbation, after which they are approximately constant, although with significant internal variability. This internal variability is reduced, but not completely eliminated, in the ensemble mean (see Fig. S1). Hence the wind stress forcing experienced by the ocean in these CRF simulations can be well-approximated by a step-function. This pattern of wind stress anomalies is indicative of a poleward shift and strengthening of the extratropical jet, giving an average positive SAM shift of about 1 standard deviation, a response which is found across a range of climate models (Seviour et al. 2017). The largest amplitude response is seen in the MITgcm ensemble, which also has a climatological wind stress maximum about 10° equatorward of the majority of other models; this is perhaps not surprising

given the idealized nature of the MITgcm simulations. The IPSL CM5A-MR wind stress maximum is also significantly equatorward of other models, a bias which was also noted in the IPSL CMIP5 simulations (Barnes and Polvani 2013) (note the observed wind stress maximum is at about 52°S [Ferreira et al. 2015], close to that in the GFDL ESM2Mc, GISS E2.1, and CCSM3.5 models). Wind stress responses in the GM200 and GM600 simulations are very similar, and their climatological wind stress maxima are almost identical, suggesting that the impact of changing A_{GM} on the atmospheric circulation and its response to ozone depletion is small.

In all models, the zonal- and annual-mean SST response to the ozone step-perturbation consists of a warming equatorward of the climatological wind stress maximum (as seen by the positive values above the dashed line in Fig. 2). This response is consistent with the decrease in wind stress in this region, leading to an anomalously poleward Ekman current. Indeed, the magnitude of this warming response appears to be related to the magnitude of the midlatitude wind stress perturbation, being largest in CCSM3.5 and MITgcm. Interestingly, this midlatitude surface warming may be transported to depth by Ekman pumping as well as enhanced ventilation and subduction, and significantly contribute towards an increase in ocean heat content (Solomon et al. 2015).

In contrast to the midlatitude response, the SST response in the SO (poleward of the wind stress maximum), which is the primary focus of this study, is much less robust among models, and is further highlighted in Fig. 3a. Within the first two years of the perturbation all models show cooling responses, but of varying magnitudes. The majority of the models then show a transition from a SO cooling to a warming over a range of time scales; we can divide these into multidecadal time scales (> 15 years: MITgcm, GFDL GM200), decadal time scales (5-15 years: GFDL GM600,

GISS E2.1), and interannual time scales (< 5 years; CCSM3.5). IPSL CM5A-MR is the only model not to show a transition from a SO cooling to warming in the annual-mean, although it has a slow warming trend in winter and spring seasons when there is little wind forcing. Since the IPSL CM5A-MR CRF simulations were only run for 25 years, it is possible that the transition may occur after this time (as it does for GFDL GM200 simulation). It is noteworthy that the two versions of the GFDL ESM2Mc model, GM200 and GM600, give very different SST responses; the GM200 ensemble has a transition from cooling to warming after about 27 years, while the GM600 has this transition after 13 years. We will return to discuss this difference in section 3c. It should also be noted that some of the initial cooling response in the GM200 ensemble is due to its ensemble average initial SST being slightly cooler than the climatological average, but that a cooling response remains once the effect of these initial conditions is removed (Seviour et al. 2016).

We may use these SST step-responses, together with Eq. 5, to infer the response to realistic time-varying ozone changes. Here we use polar cap (60-90°S) averaged column ozone from a transient simulation of the Whole Atmosphere Chemistry-Climate Model (WACCM), from 1955-2020 (inset, Fig. 3b). This provides ozone changes which are in close agreement with observed values (Froidevaux et al. 2018). The WACCM simulations follow the REF-C2 scenario specified by the Chemistry-Climate Model Initiative (CCMI), using observed forcings up to 2005, and following the RCP6.0 scenario thereafter. The column ozone time series is smoothed using a decadal running mean. It is first necessary to scale each CRF by the ozone perturbation for each model; for the case of MITgcm, in which ozone is not explicitly represented, we assume the change is equivalent to the change in WACCM between the years 1960 and 2000. Additionally, we must extrapolate the CRFs such that they are 65 years long (the same length as the ozone signal) in order to be able to

perform the full convolution in Eq. 5. To do so we simply assume that the CRF stays at a constant equal to its value in its final year up to year 65 (i.e. we extrapolate a horizontal line from the final value to year 65).

A wide range of predicted forced responses to realistic ozone changes is seen among the different models (Fig. 3b). Even though almost all models show a two-time-scale response with an initial cooling in their CRFs, some models show a monotonic warming in response to realistic ozone changes (CCSM3.5, GFDL GM600), with no cooling period. Note that this model spread is clearly evident at 1980, before any extrapolation beyond the length of CRF simulations is needed. The observed trend in annual-mean SO SST (Fig. S2) consists of a warming of approximately 0.15 K from the 1950s until about 1980 (though with large observational uncertainty), followed by a cooling of similar magnitude through 2016 (Fan et al. 2014, Jones et al. 2016). All models show small SST changes from the 1950s to 1970s because the change in ozone forcing is small over this period. The only model to replicate a similar (though weaker in magnitude) multidecadal cooling trend from 1980 is IPSL CM5A-MR, which does not have a two-time-scale CRF (or has a second time scale which is too long to be captured by the CRF simulations). Even models with a multidecadal cooling in their CRF (MITgcm, GFDL GM200) show a transition to a warming trend in the 1990s. This finding is in agreement with Kostov et al. (2018), who showed that inferred SAM CRFs (as described in section 2b) convolved with observed SAM trends fail to replicate the SST cooling from 1980 in the vast majority of CMIP5 models. They found that it was only possible to replicate a SST trend as large as observed in those models with a very long transition time scale. In the next section we explicitly compare these inferred SAM CRFs with the fully-nonlinear ozone CRFs in each of our six models.

b. Comparison of SAM and ozone CRFs

SAM CRFs, as described in section 2b, represent the predicted SO SST response to a 1 standard deviation perturbation to the SAM, inferred through lagged linear regression (Kostov et al. 2017). In order to make a direct comparison with the ozone CRFs described in the previous section, we scale the SAM CRF by the SAM perturbation (measured in standard deviations) induced by ozone depletion in each model's ozone CRF experiments. For the GFDL GM200 and 600, and IPSL CM5A-MR this is less than one standard deviation, leading to a reduction in the magnitude of the SAM CRF, while for CCSM3.5 the scaling is greater than one standard deviation. The comparison of ozone CRFs and scaled SAM CRFs (with uncertainties calculated as described in section 2b) is shown in Fig. 4. For all models, with the exception of GFDL GM200, the SAM CRF consists of a cooling followed by a warming. For GFDL GM200 the SAM CRF is a monotonic cooling, however, with much larger uncertainty than the other models. The source of this large uncertainty lies in the fact that the GFDL GM200 simulation displays quasi-periodic deep convective events in the SO, leading to periodicity and therefore autocorrelation in SSTs (Seviour et al. 2016, Cabré et al. 2017). Due to this quasi-periodic internal variability, it is not straightforward to estimate the uncertainty in the ozone CRF from the ensemble spread, since this is dominated by differences in ensemble member initial conditions (Seviour et al. 2016). Therefore, the ozone CRF uncertainty ranges in Fig. 4 are estimated as the standard deviation of the ensemble mean after subtracting a 15-year running mean.

Except for the GFDL GM200 model for time scales longer than 20 years, there is reasonably good agreement between the SAM and ozone CRFs. If, as with the ozone CRFs, we divide the SAM CRF cooling responses into multidecadal (MITgcm), decadal (GFDL GM200, GISS E2.1), and interannual (CCSM3.5, IPSL CM5A-MR) time scales, we see that models fall into the same groupings under both approaches (the only exception being IPSL CM5A-MR for which the sign of the two CRFs disagrees after 5 years, although both responses are very weak). It is particularly noteworthy that the SAM CRFs also pick up on the large difference between GFDL GM200 and GM600 responses.

The SAM CRFs computed for the 6 models considered here can be compared with SAM CRFs calculated by Kostov et al. (2018) for 19 models from the CMIP5 ensemble (Fig 5; note this shows the unscaled SAM CRFs). The GFDL GM200 model appears an outlier from the CMIP5 spread, however the one CMIP5 model with a similar strong cooling response is GFDL CM3, indicating that this response may be a feature of the GFDL model family, and potentially related to their quasi-periodic SO variability. The GFDL GM200 and GM600 SAM CRFs approximately span the entire range of CMIP5 responses, indicating a strong effect of altering the eddy advection parameterization. A third, intermediate GFDSL ESM2Mc case, GM400 (minimum A_{GM} = 400 m^2s^{-1}) is also shown in Fig 5, and its CRF lies between the other two. In the next section we focus on understanding the relationship between models' CRFs and their climatology. Since we have shown that ozone and SAM CRFs give broadly similar results, we hereafter focus on SAM CRFs, allowing for comparison of a wider range of models.

c. Relationship between CRFs and model climatology

368

369 The GFDL ESM2Mc experiments with differing Gent-McWilliams coefficients, A_{GM}, allow us to
370 probe the relationship between a model's climatology and its response to ozone depletion.
371 Increasing A_{GM} leads to a flattening of isopycnals (Gent et al. 1995). In the Southern Ocean, where
372 isopycnals slope up to the surface, the effect of increasing A_{GM} is therefore to reinforce the vertical
373 density gradient, allowing for a stronger temperature inversion, as can be seen in Fig. 6a. In GFDL
374 ESM2Mc, increasing the A_{GM} minimum value from 200 to 600 m^2s^{-1} leads to an increase in the
375 climatological annual mean temperature inversion, $\boldsymbol{\Delta}_z[\theta]$ (defined as the maximum vertical
376 temperature contrast in the upper 500 m) from 1.3 K to 2.2 K. Interestingly, another impact of
377 increasing A_{GM} is to inhibit SO deep convective variability (Thomas et al. 2018). In the standard
378 GM200 case, quasi-periodic deep convective variability leads to changes in annual mean SO (50-
379 70°S*)* SST of up to 2 K, on time scales of approximately 50 years (Fig. 6b, purple line). For the
380 higher mixing, GM600 case, there is no clear multidecadal variability and changes annual mean
381 SO SST are less than 1 K (orange line). The intermediate GM400 control case is also shown in
382 Fig. 6b (green line), and can be seen to have some decadal variability, though with a lower
383 magnitude than the GM200 case.
384

385 Kostov et al. (2017) showed that the strength of the year-1 cooling, and the rate of the subsequent
386 warming (years 1-7) among CMIP5 SAM CRFs are correlated with the model's climatological
387 meridional SST gradient and vertical temperature inversion respectively. These relationships are
388 again shown in Fig. 7 (gray points). Note that the data shown is not identical to Kostov et al. (2017)
389 because we here consider the response to a December-May SAM perturbation (to make a closer
390 link with the ozone response), while Kostov et al. (2017) considered an annual-mean perturbation;

391 however, the relationships are very similar in the two cases. The linear fits shown in Fig. 7 are
392 calculated by weighting each model by the inverse square of its uncertainty. While both slopes
393 significantly differ from zero (according to a two-tailed t-test at the 95% confidence level), it is
394 clear that the relationships fail to explain a large fraction of the inter-model spread; R^2 values are
395 just 0.52 and 0.20 for the fast and slow responses respectively. This is perhaps not surprising given
396 the large number of differences between CMIP5 models which could affect the SST response to
397 the SAM.
398
399 The perturbed Gent-McWilliams coefficient GFDL ESM2Mc simulations can be used as a 'clean
400 experiment' to test the CMIP5 climatology-response relationships. Any differences between the
401 SAM CRFs of these simulations can be unambiguously attributed to the change in eddy
402 parameterization and its subsequent effect on the ocean climatology; other significant factors (e.g.
403 atmospheric dynamics, cloud feedbacks, sea-ice parameterization) remain constant. Altering the
404 A_{GM} has little effect on the climatological meridional SST gradient, and, consistent with Kostov et
405 al. (2017), the fast time scale responses of all three cases agree to within error (Fig. 7a, colored
406 points). However, as discussed above, a higher A_{GM} leads to a stronger temperature inversion, so
407 given the relationship among CMIP5 models, we would expect a faster warming rate for higher
408 A_{GM}. This is indeed found (Fig. 7b). The difference among the warming rates of the three A_{GM}
409 cases is slightly greater than would be predicted from the CMIP5 regression, although the
410 regression coefficients agree to within error. This result lends support that correlations found by
411 Kostov et al. (2017) are indeed causal relationships.
412

An additional factor which may contribute to the large inter-model spread in SAM CRFs is differences in cloud-circulation feedbacks and their subsequent impact on shortwave radiation. Grise and Polvani (2014) studied cloud-radiative anomalies associated with shifts in the latitude of the Southern Hemisphere extratropical jet among CMIP5 models. They quantified this effect through a jet-cloud radiative effect (CRE) index; defined as the change in CRE averaged over 30-60°S associated with a 1° poleward shift of the jet, where the CRE is the change in top-of-atmosphere outgoing radiation between clear-sky and all-sky scenarios (Ramanathan et al. 1989). CMIP5 models can be divided into two groups; those for which a poleward shift of the jet leads to a reduction in midlatitude cloud fraction and a subsequent shortwave surface warming (jet-CRE index > 0), and those for which this warming effect is largely absent (jet-CRE index < 0). Seviour et al. (2017) showed that a reduction in shortwave heating plays an important role in driving the short-term SST cooling response to ozone depletion in GFDL ESM2Mc. Motivated by this result we here show the relationship between CMIP5 models' December-March jet-CRE indices and their year-1 SST cooling in the SAM CRF (Fig. 8a). A positive correlation, which statistically significant (at the 95% level), can be seen. Although the R^2 value of 0.15 is less than those in Fig. 7, the sign of the correlation is physically intuitive. Models with a positive jet-CRE index display a shortwave warming associated with a poleward jet shift (positive SAM) which opposes the SST cooling response. Models with a negative jet-CRE index have a net shortwave cooling associated with the SAM perturbation, leading to a stronger SST cooling. Following Grise and Polvani (2014), two observational jet-CRE index estimates are indicated in Fig. 8a. These are both negative (-0.5 W m^{-2} for ISCCP-FD, and -0.34 W m^{-2} for CERES), thereby favoring a stronger short-term cooling response to the SAM perturbation.

Complicating the relationship shown in Fig 8a, is the fact that CMIP5 models' jet-CRE indices and their background SST gradients are themselves statistically significantly correlated (Fig. 8b). Models with a negative jet-CRE index generally have a stronger SST gradient than those with a positive jet-CRE index. It is therefore unclear whether the relationship shown in Fig. 8a is causal, meaning jet-CRE feedbacks directly affect the SST response to SAM. To test the causality of the relationship it will be necessary to construct an experiment in which only cloud feedbacks are perturbed, without changing the SST climatology; a similar approach to the perturbed A_{GM} experiments described above.

4. Discussion and implications for sea ice

A major motivation for this study has been understanding the extent to which ozone depletion may have contributed towards the surprising multidecadal cooling of SO SST since about 1980 (Fan et al. 2014; Fig. S2). We have shown that even models with a long (~30 year) SST cooling response to a step ozone perturbation do not predict a cooling from 1980-present in response to realistic ozone changes, rather they show a warming trend from at least as early as the mid-1990s (Fig. 3). Hence, if ozone depletion were to be the driving the observed SST trend, then the climate system must exhibit a cooling phase that is longer than that of any of the models, or have a monotonic cooling response, with no long term warming. However, the position of the observed SO climatology among the climatology-response relationships shown in Fig. 7b indicates that this is unlikely to be the case. The observed estimate for the strength of the SO temperature inversion lies towards the middle of the CMIP5 model spread, and between the GM200 and GM400 GFDL ESM2Mc experiments. This favors a slightly positive SST trend over years 1-7 following the step

perturbation, not the cooling that would be needed to reproduce the observed SST trend. However, it is of course possible that the climate system is an outlier from the relationship shown in Fig. 7b, possessing a stronger long-term cooling response than would be expected from its climatological temperature inversion. Indeed, this might be the case if eddy compensation counteracts the wind-driven upwelling of warm subsurface water (Doddridge et al. 2019), a process which may not be well-captured by the models analyzed here.

An alternative explanation for the observed SST cooling is that it is the result of other processes or internal climate variability. It should be noted that this internal variability would have to be sufficiently strong to overcome both the likely warming trend induced by ozone depletion, as well as the warming effect of rising greenhouse gas concentrations. Kostov et al. (2018) estimated this greenhouse gas-driven warming of SO SST to be approximately 0.04 °C decade^{-1} over 1979-2014 . We have shown here that models vary greatly in their magnitudes and time scales of SO internal variability, and that this variability is highly sensitive to the parameterization of subgrid-scale mixing (Fig. 6). The most variable GFDL ESM2Mc experiment (GM200) showed SO SST changes of nearly 2 K over periods of about 50 years. However, even the least variable case (GM600) has changes of about 0.5 K over 50 years. Such changes would be more than sufficient to explain the observed 30-year cooling of about 0.15 K since 1980.

We have focused exclusively on the SST response to ozone depletion and so have not presented a detailed discussion of accompanying sea-ice changes. However, it might be assumed that there is a strong relation between the two quantities; that models which have a stronger SST cooling response show a greater sea-ice expansion. Responses of summer and winter sea-ice extent are

shown for each of the ozone CRF experiments in Fig. 9., revealing that the SST-sea-ice relationship is not so straightforward. In fact, only one model shows a sea-ice expansion beyond the first year after ozone depletion in either the summer or winter (MITgcm), despite the fact that most models show a 50-70°S average SST cooling lasting several years.

This apparent conflict between SST and sea-ice changes may result from SST changes being largely equatorward of the sea-ice edge (as shown by Seviour et al. (2016) for GFDL ESM2Mc), or from zonal asymmetries in the SST response. Indeed, it should be noted that the small yet significant observed Antarctic sea-ice expansion over recent decades is the result of two almost-cancelling regional trends, with the largest expansion in the Ross Sea, and the largest decline in the Bellingshausen and Amundsen seas (Hobbs et al., 2016). Following a similar approach to Kostov et al. (2017), Holland et al. (2016) used lagged linear regression to investigate the response of sea-ice extent to a step SAM perturbation in the CMIP5 ensemble. They found that the majority of models exhibit a two-time-scale response, with an initial sea-ice expansion followed by a decline. The fact that this two-time-scale is only seen in one ozone CRF experiment (for the nearly zonally-symmetric MITgcm) suggests that the relationship between ozone and SAM CRFs may be less strong in the case of sea-ice, potentially the result of regional impacts of ozone depletion which do not project on to the SAM.

5. Conclusions

Here we have examined the impact of ozone depletion on SO SST, with a particular emphasis on the time-dependence of the response through the calculation of CRFs; responses to instantaneous

505 step-changes in forcing. Our synthesis of recently-published studies, alongside several new
506 simulations has revealed that:
507
508 1. Two recent approaches for estimating the transient impact of ozone depletion on Southern
509 Ocean SST broadly agree on the time scales and magnitudes of the response. The first
510 approach simulates the fully-nonlinear CRF for an explicit ozone perturbation (Ferreira et
511 al. 2015; Seviour et al. 2016, 2017), while the second infers the CRF through lagged linear
512 regression of the SAM and SST (Kostov et al. 2017; 2018). Note that it is not immediately
513 obvious that these two approaches should have given similar results since the linear
514 approach neglects potentially important feedbacks between the SAM and SST, and
515 assumes that the tropospheric response to ozone depletion can be approximated by a SAM
516 perturbation.
517
518 2. While almost all models show a two-time-scale response to an ozone perturbation,
519 consisting of a short-term cooling followed by a long-term warming, we find large inter-
520 model spread (duration of cooling ranges from 2 years to 30 years). When considering the
521 SST response to realistic time-varying ozone changes, this CRF uncertainty results in an
522 uncertainty even as to the sign of the response (i.e. whether it is a cooling or a warming).
523
524 3. We provide further evidence to support the finding of Kostov et al. (2017), that biases
525 among models' CRFs are related to biases in their SO climatology, with the short term
526 response being related to the meridional SST gradient, and the long-term response related
527 to the strength of the SO temperature inversion. Experiments with perturbed subgrid-scale

mixing (Gent-McWilliams parameter minimum) confirm this relationship, and highlight that a perturbation to a single parameter within a single model can cause a change to the CRF which approximately spans the range of CMIP5 responses. Cloud-circulation feedbacks may also play a significant role in model CRF biases, but since they are also related to the SO climatology, untangling these effects is not straightforward.

4. Combining the climatology-response relationship in models with observed climatological values allows us to constrain the likely forced response of the real climate system. Although there are significant uncertainties, such an analysis suggests that ozone depletion is unlikely to have driven the observed SO SST cooling trend over 1980-present. Many models produce internal multidecadal SO SST trends of sufficient magnitude to explain the observed trend.

While the climatology-response relationships shown in Figs. 7 and 8 have gone some way to understanding the large diversity of model CRFs, it is clear that a significant fraction of the inter-model variance remains unexplained. It is challenging to pin-down the causes of uncertainty in multi-model ensembles because many factors differ between models. Using the perturbed-A_{GM} experiments shown here we were able to unambiguously attribute one potential driver of inter-model diversity. Extending this approach to other important processes (e.g. cloud feedbacks, air-sea heat fluxes, sea-ice) provides a way forward for understanding and reducing inter-model uncertainty.

Acknowledgements

This work was supported by the National Science Foundation under NSF proposal FESD-1338814. Data from the CRF simulations analyzed here is available from the authors on request. CMIP5 data used in this study is freely available through the Earth System Grid Federation (https://esgf-node.llnl.gov).

References

Armour K. C. and C. M. Bitz (2016) Observed and projected trends in Antarctic sea ice. US CLIVAR Var 13(4):13–19

Barnes, E.A. and L. M. Polvani (2013), Response of the Midlatitude Jets, and of Their Variability, to Increased Greenhouse Gases in the CMIP5 Models. *J. Climate*, 26, 7117–7135, doi:10.1175/JCLI-D-12-00536.1

Bitz, C. M., and L. M. Polvani (2012), Antarctic climate response to stratospheric ozone depletion in a fine resolution ocean climate model, *Geophys. Res. Lett.*, 39, L20705, doi: 10.1029/2012GL053393.

Cabré, A., I. Marinov and A. Gnanadesikan (2017), Global atmospheric teleconnections and multi-decadal climate oscillations driven by Southern Ocean convection, *J. Climate,* 30, 8107-8126, doi:10.1175/JCLI-D-16-0741.1

Ciasto, L.M. and D.W. Thompson (2008), Observations of Large-Scale Ocean–Atmosphere Interaction in the Southern Hemisphere. *J. Climate*, 21, 1244–1259, doi:10.1175/2007JCLI1809.1

573 Cionni, I., V. Eyring, J. F. Lamarque, W. J. Randel, D. S. Stevenson, F. Wu, G. E. Bodeker, T.
574 G. Shepherd, D. T. Shindell, and D. W. Waugh (2011), Ozone database in support of CMIP5
575 simulations: results and corresponding radiative forcing, *Atmos. Chem. Phys.*, 11, 11267-
576 11292. doi:10.5194/acp-11-11267-2011.
577 Doddridge, E. W., J. Marshall, H. Song, M. Kelley, and L. Nazarenko (2019), Eddy
578 compensation dampens Southern Ocean SST response to westerly wind trends, *Geophys.*
579 *Res. Lett.,* 46, doi:10.1029/2019GL082758
580 Dufresne et al. (2013) Climate change projections using the IPSL-CM5 Earth System Model:
581 from CMIP3 to CMIP5. *Clim. Dyn.,* 40, 2123–2165. doi:10.1007/s00382-012-1636-1
582 Fan T., C. Deser and D. P. Schneider (2014) Recent Antarctic sea ice trends in the context of
583 Southern Ocean surface climate variations since 1950. *Geophys. Res. Lett.* 41, 2419–2426.
584 doi: 10.1002/2014GL059239
585 Ferreira, D., J. Marshall, C.M. Bitz, S. Solomon, and A. Plumb (2015), Antarctic Ocean and Sea
586 Ice Response to Ozone Depletion: A Two-Time-Scale Problem. *J. Climate*, 28, 1206–1226,
587 doi:10.1175/JCLI-D-14-00313.1
588 Froidevaux, L., D. E. Kinnison, R. Wang, J. Anderson and R. A. Fuller (2018), Evaluation of
589 CESM1 (WACCM) free-running and specified-dynamics atmospheric composition
590 simulations using global multi-species satellite data records, Atmos. Chem. Phys. Discuss.
591 doi:10.5194/acp-2018-546
592 Gent, P.R. and J.C. McWilliams (1990), Isopycnal Mixing in Ocean Circulation Models. *J. Phys.*
593 *Oceanogr.*, 20, 150–155.
594 Gent, P.R., J. Willebrand, T.J. McDougall, and J.C. McWilliams (1995), Parameterizing Eddy-
595 Induced Tracer Transports in Ocean Circulation Models. *J. Phys. Oceanogr.*, 25, 463–474.

596 Gerber, E.P. and S. Son (2014) Quantifying the Summertime Response of the Austral Jet Stream
597 and Hadley Cell to Stratospheric Ozone and Greenhouse Gases. *J. Climate*, 27, 5538–5559,
598 doi:10.1175/JCLI-D-13-00539.1.
599 Good SA, Martin MJ, Rayner NA (2013) EN4: quality controlled ocean temperature and salinity
600 profiles and monthly objective analyses with uncertainty estimates. J *Geophys Res* 118,
601 6704–6716. doi: 10.1002/2013JC009067
602 Goosse, H., W. Lefebvre, A. de Montety, E. Crespin, and A. H. Orsi (2009): Consistent past
603 half-century trends in the atmosphere, the sea ice and the ocean at high southern latitudes.
604 Climate Dyn., 33, 999–1016, doi:10.1007/s00382-008-0500-9
605 Grise, K. M. and L. M. Polvani (2014) Southern Hemisphere Cloud–Dynamics Biases in CMIP5
606 Models and Their Implications for Climate Projections. *J. Climate*, 27, 6074–6092,
607 doi:10.1175/JCLI-D-14-00113.1
608 Hall, A. and M. Visbeck (2002) Synchronous Variability in the Southern Hemisphere
609 Atmosphere, Sea Ice, and Ocean Resulting from the Annular Mode. *J. Climate*, 15, 3043–
610 3057.
611 Hande, L. B., S. T. Siems, and M. J. Manton (2012), Observed Trends in Wind Speed over the
612 Southern Ocean, *Geophys. Res. Lett.*, 39, L11802, doi: 10.1029/2012GL051734.
613 Hobbs, W. R., R. Massom, S. Stammerjohn, P. Reid, G. Williams, W. Meier, A review of recent
614 changes in Southern Ocean sea ice, their drivers and forcings, (2016). *Global and Planetary*
615 *Change*, 143, 228-250 doi:10.1016/j.gloplacha.2016.06.008.
616 Hasselmann, K., (1993) Optimal Fingerprints for the Detection of Time-dependent Climate
617 Change. *J. Climate*, 6, 1957–1971

618 Holland, M. M., L. Landrum, Y. Kostov, and J. Marshall (2016), Sensitivity of Antarctic sea ice
619 to the Southern Annular Mode in coupled climate models, Clim. Dyn., 49, 1813-1831,
620 doi:10.1007/s00382-016-3424-9.
621 Jones, J. M., S. T. Gille, H. Goosse, N. J. Abram, P. O. Canziani, D. J. Charman, K. R. Clem, X.
622 Crosta, C. de Lavergne, I. Eisenman, M. H. England, R. L. Fogt, L. M. Frankcombe, G. J.
623 Marshall, V. Masson-Delmotte, A. K. Morrison, A. J. Orsi, M. N. Raphael, J. A. Renwick,
624 D. P. Schneider, G. R. Simpkins, E. J. Steig, B. Stenni, D. Swingedouw and T. R. Vance
625 (2016), Assessing recent trends in high-latitude Southern Hemisphere surface climate, Nat.
626 Climate Change, 6, 917-926, doi:10.1038/nclimate3103
627 Kostov, Y., J. Marshall, U. Hausmann, K. C. Armour, D. Ferreira and M. M. Holland (2017)
628 Fast and slow responses of Southern Ocean sea surface temperature to SAM in coupled
629 climate models, *Clim. Dyn*. 48: 1595-1609, doi:10.1007/s00382-016-3162-z.
630 Kostov, Y., Ferreira, D., Armour, K. C., and Marshall, J. (2018). Contributions of greenhouse
631 gas forcing and the Southern Annular Mode to historical Southern Ocean surface
632 temperature trends. Geophys. Res. Lett., 45, 1086–1097 doi:10.1002/2017GL074964
633 Loeb, N. G., S. Kato, W. Su, T. Wong, F. G. Rose, D. R. Doelling, J. R. Norris, and X. Huang
634 (2012) Advances in understanding top-of-atmosphere radiation variability from satellite
635 observations. *Surv. Geophys.*, 33, 359–385, doi:10.1007/ s10712-012-9175-1.
636 Marsh, D.R., M.J. Mills, D.E. Kinnison, J. Lamarque, N. Calvo, and L.M. Polvani (2013),
637 Climate Change from 1850 to 2005 Simulated in CESM1(WACCM). *J. Climate*, 26, 7372–
638 7391, doi:0.1175/JCLI-D-12-00558.1
639 Marshall J., K. C. Armour, J. R. Scott, Y. Kostov, U. Hausmann, D. Ferreira, T. G. Shepherd and
640 C. M. Bitz (2014), The ocean's role in polar climate change: asymmetric Arctic and

Antarctic responses to greenhouse gas and ozone forcing, *Phil. Trans. R. Soc. A*, 372, 20130040; doi:10.1098/rsta.2013.0040.

Meehl, G. A., J. M. Arblaster, C. T. Y. Chung, M. M. Holland, A. DuVivier, L. Thompson, D. Yang, C. M. Bitz (2019), Sustained ocean changes contributed to sudden Antarctic sea ice retreat in late 2016, Nat. Commun., 10, 14, doi:10.1038/s41467-018-07865-9

Polvani, L.M., D.W. Waugh, G.J. Correa, and S. Son (2011) Stratospheric Ozone Depletion: The Main Driver of Twentieth-Century Atmospheric Circulation Changes in the Southern Hemisphere. J. Climate, 24, 795–812, doi:10.1175/2010JCLI3772.1

Previdi, M. and Polvani, L. M. (2014), Climate system response to stratospheric ozone depletion and recovery. Q.J.R. Meteorol. Soc., 140: 2401-2419. doi:10.1002/qj.2330

Ramanathan, V., R. D. Cess, E. F. Harrison, P. Minnis, B. R. Barkstrom, E. Ahmad, and D. Hartmann (1989) Cloud radiative forcing and climate: Results from the Earth Radiation Budget Experiment. Science, 243, 57–63, doi:10.1126/science.243.4887.57.

Reynolds RW, Rayner NA, Smith TM, Stokes DC, Wang W (2002) An improved in situ and satellite SST analysis for climate. *J Climate*, 15, 1609–1625

Seviour, W.J.M., A. Gnanadesikan, and D.W. Waugh (2016) The Transient Response of the Southern Ocean to Stratospheric Ozone Depletion. *J. Climate*, 29, 7383–7396, doi:10.1175/JCLI-D-16-0198.1

Seviour, W. J. M., A. Gnanadesikan, D. W. Waugh, and M.-A. Pradal (2017) Transient Response of the Southern Ocean to Changing Ozone: Regional Responses and Physical Mechanisms. *J. Climate*, 30, 2463–2480, doi:10.1175/JCLI-D-16-0474.1

662 Seviour, W. J. M., D. W. Waugh, L. M. Polvani, G. J. Correa, and C. I. Garfinkel (2017)
663 Robustness of the Simulated Tropospheric Response to Ozone Depletion. *J. Climate*, 30,
664 2577–2585, doi:10.1175/JCLI-D-16-0817.1
665 Sigmond, M., and J. C. Fyfe (2010), Has the ozone hole contributed to increased Antarctic sea
666 ice extent? *Geophys. Res. Lett.*, 37, L18502, doi: 10.1029/2010GL044301.
667 Sigmond, M. and J. C. Fyfe (2014) The Antarctic Sea Ice Response to the Ozone Hole in
668 Climate Models. *J. Climate*, 27, 1336–1342, doi:10.1175/JCLI-D-13-00590.1
669 Smith, K. L., L. M. Polvani, and D. R. Marsh (2012), Mitigation of 21st century Antarctic sea ice
670 loss by stratospheric ozone recovery, *Geophys. Res. Lett.*, 39, L20701, doi:
671 10.1029/2012GL053325.
672 Solomon, A., L. M. Polvani, K. L. Smith, and R. P. Abernathey (2015), The impact of ozone
673 depleting substances on the circulation, temperature, and salinity of the Southern Ocean: An
674 attribution study with CESM1(WACCM), *Geophys. Res. Lett.*, 42, 5547–5555, doi:
675 10.1002/2015GL064744.
676 Swart, N. C., and J. C. Fyfe (2012), Observed and simulated changes in the Southern
677 Hemisphere surface westerly wind-stress, *Geophys. Res. Lett.*, 39, L16711, doi:
678 10.1029/2012GL052810.
679 Swart, N.C., J.C. Fyfe, N. Gillett, and G.J. Marshall (2015) Comparing Trends in the Southern
680 Annular Mode and Surface Westerly Jet. *J. Climate*, 28, 8840–8859, doi:10.1175/JCLI-D-
681 15-0334.1
682 Thomas, J. L., D. W. Waugh, and A. Gnanadesikan (2015), Southern Hemisphere extratropical
683 circulation: Recent trends and natural variability, *Geophys. Res. Lett.*, 42, 5508–5515, doi:
684 10.1002/2015GL064521.

Thomas, J., D. Waugh, and A. Gnanadesikan (2018) Relationship between Ocean Carbon and Heat Multidecadal Variability. *J. Climate*, 31, 1467–1482, doi:10.1175/JCLI-D-17-0134.1

Thompson, D. W. J. and S. Solomon (2002). Interpretation of Recent Southern Hemisphere Climate Change, *Science*, 296, 895-899, doi:10.1126/science.1069270

Thompson, D. W. J., Solomon, S., Kushner, P. J., England, M. H., Grise, K., Karoly, D. J., (2011) Signatures of the Antarctic ozone hole in Southern Hemisphere surface climate change. *Nat. Geosci.* 4, 741-749, doi:10.1038/ngeo1296.

Zhang, Y. C., W. B. Rossow, A. A. Lacis, V. Oinas, and M. I. Mishchenko (2004) Calculation of radiative fluxes from the surface to top of atmosphere based on ISCCP and other global data sets: Refinements of the radiative transfer model and the input data. J. Geophys. Res., 109, D19105, doi:10.1029/2003JD004457

Tables

Model	Ensemble size	Simulation length	Reference
MITgcm	20	40 years	Ferreira et al. 2015
CCSM3.5	6 (+20 for first 32 months)	20 years	Ferreira et al. 2015
GISS E2.1	8	60 years	Doddridge et al. 2019
GFDL ESM2Mc (GM200)	24	45 years	Seviour et al. 2016
GFDL ESM2Mc (GM600)	12	45 years	This study
IPSL CM5A-MR	24	25 years	This study

Table 1: Models for which ozone depletion CRF simulations have been performed.

719

720

721 **Figures**

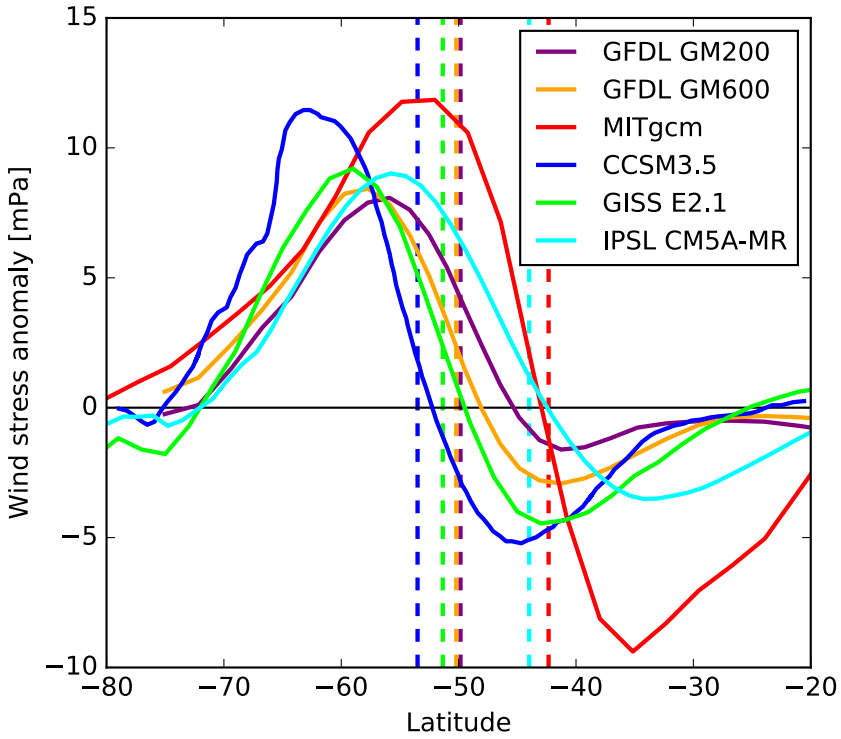

722

723 *Figure 1: Ensemble-mean, annual-mean, zonal-mean zonal wind stress anomalies in the ozone*
724 *CRF simulations of 6 models. Dashed vertical lines indicate the latitude of maximum wind stress*
725 *in the control simulation of each model.*

726

727

728

729

730

731

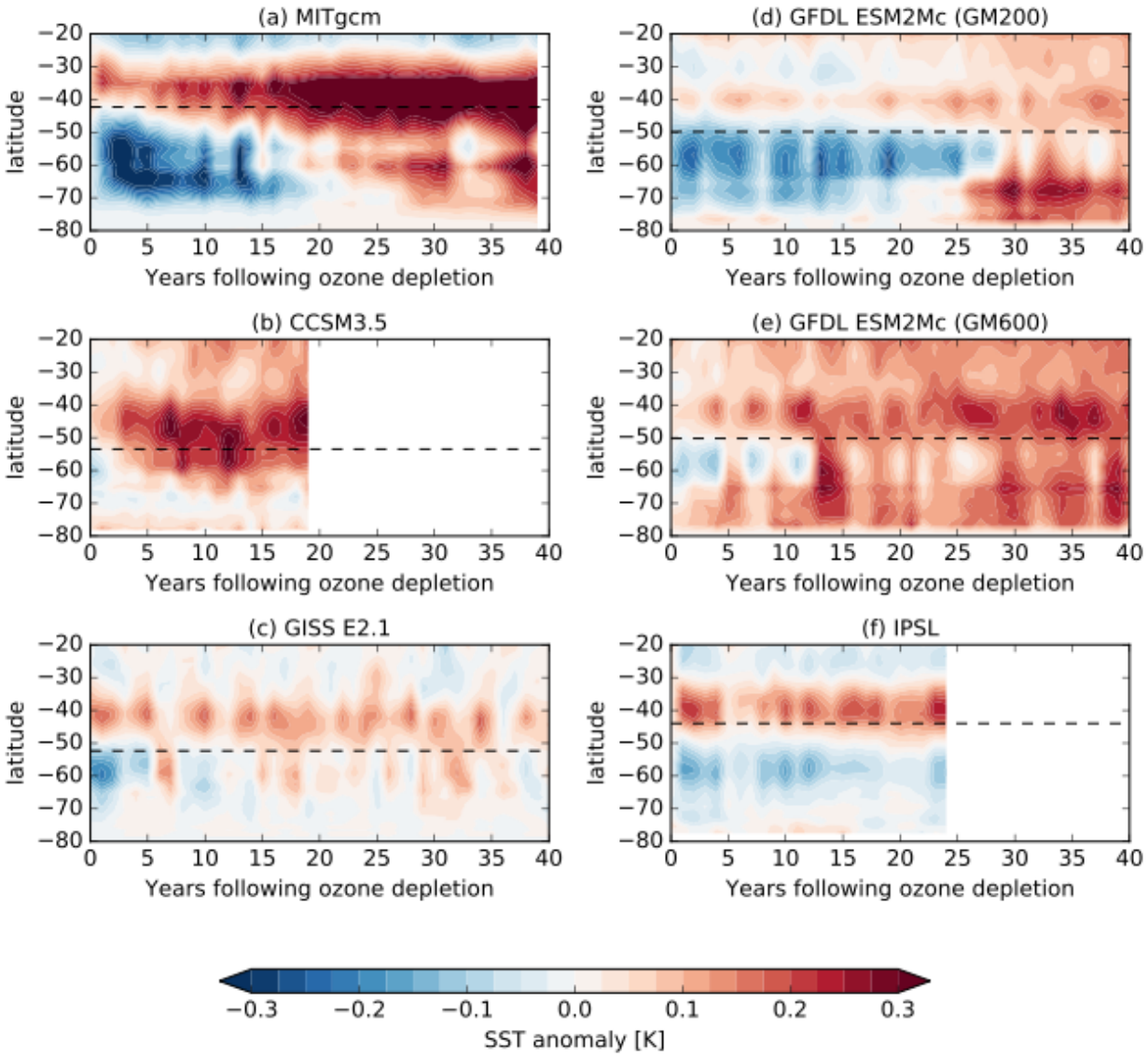

732

733 *Figure 2: Ensemble mean, annual-mean, zonal-mean SST anomalies in the ozone CRF*

734 *simulations of 6 models. Dashed horizontal lines indicate the latitude of maximum zonal wind*

735 *stress in the control simulation of each model (as in Fig. 1).*

736

737

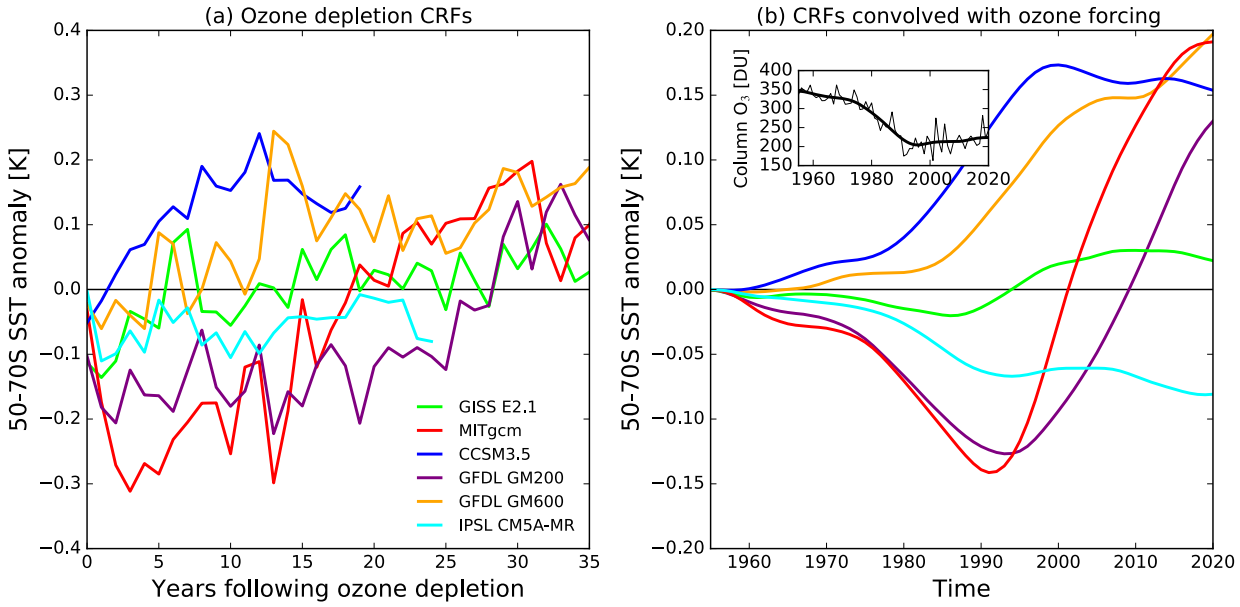

738

739 *Figure 3: (a) Ensemble-mean time series of annual-mean SST averaged over the Southern Ocean*

740 *region (50-70°S) in each ozone CRF simulation. (b) Convolution of SST CRFs in (a) with ozone*

741 *forcing (inset figure, showing October-mean polar cap (60-90°S) column ozone) from 1955 to*

742 *give the predicted forced SST response to the time-varying ozone forcing. The ozone forcing is*

743 *taken from a simulation of the WACCM chemistry-climate model.*

744

745

746

747

748

749

750

751

752

753

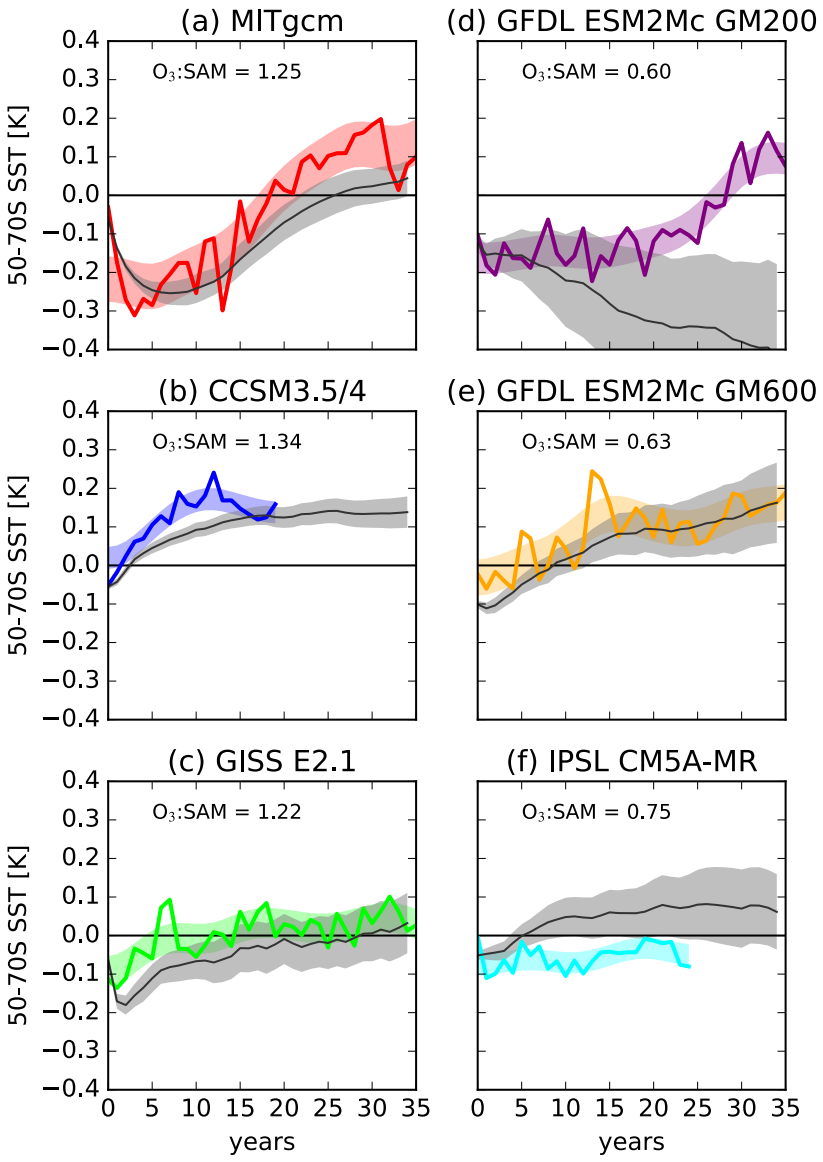

754

755 *Figure 4: Comparison of ozone CRFs and inferred SAM CRFs. Colored lines show the 50-70°S*
756 *annual mean SST response to step ozone depletion for each model, as in Fig 1. Thin black lines*
757 *show the inferred SST response to a 1σ SAM step perturbation over December-May, derived*
758 *from the control simulation of each model. In order to make the SAM and ozone responses*
759 *directly comparable in magnitude, the SAM responses have been scaled by the SAM perturbation*
760 *in each ozone CRF simulation (measured in standard deviations). This scaling is shown in the*
761 *upper left of each plot. Shaded regions show ± 1 standard error in the CRFs.*

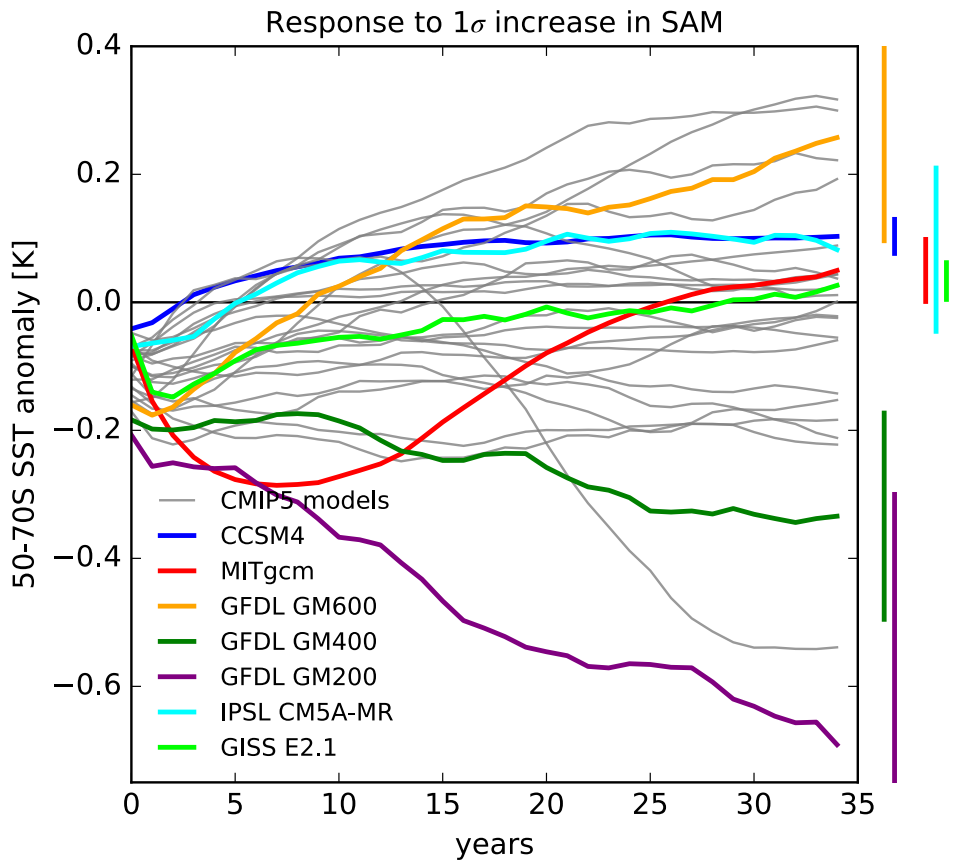

762

763 *Figure 5: Response of 50-70°S annual-mean SST to a 1σ step perturbation in the December-May*

764 *SAM, derived from model control simulations. Colored lines show the models for which ozone*

765 *depletion CRFs have been calculated. Gray lines show the 19 CMIP5 simulations (data from*

766 *Kostov et al. 2018). Bars at the right hand side show the ± 1 standard error uncertainty at year*

767 *35.*

768

769

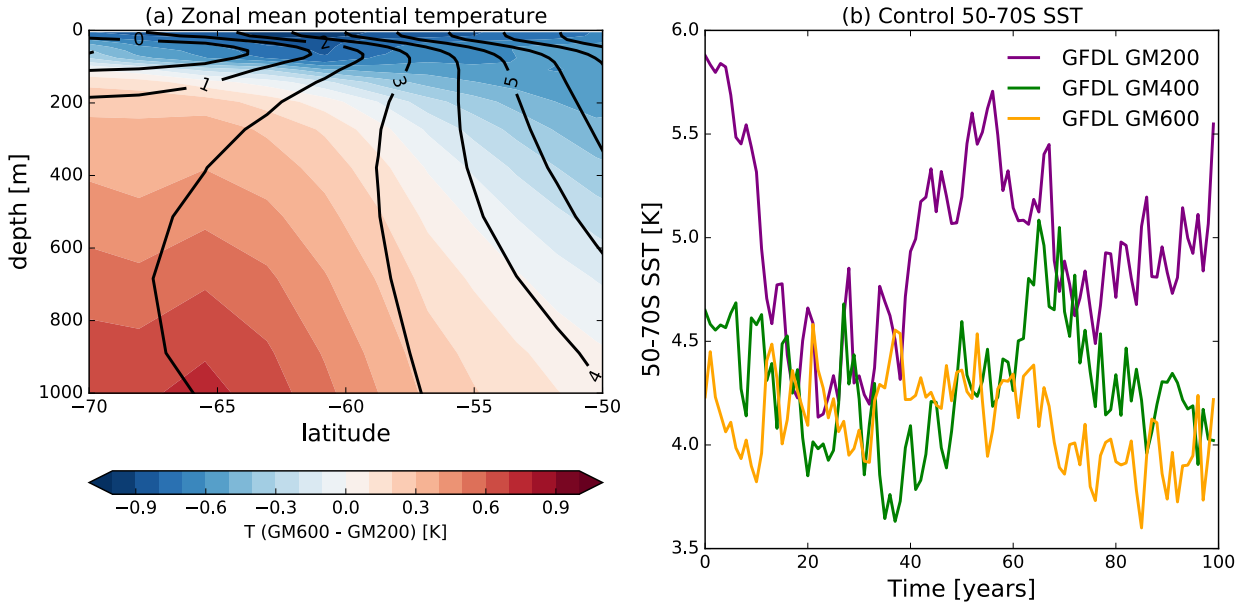

Figure 6: Comparison of GFDL ESM2Mc control simulations with different GM parameter minimum values. (a) Zonal-mean potential temperature for the GM200 simulation (black contours, °C) and anomalies of the GM600 simulation relative to GM200 (colors). (b) Time series of 100 years of 50-70°S annual-mean SST.

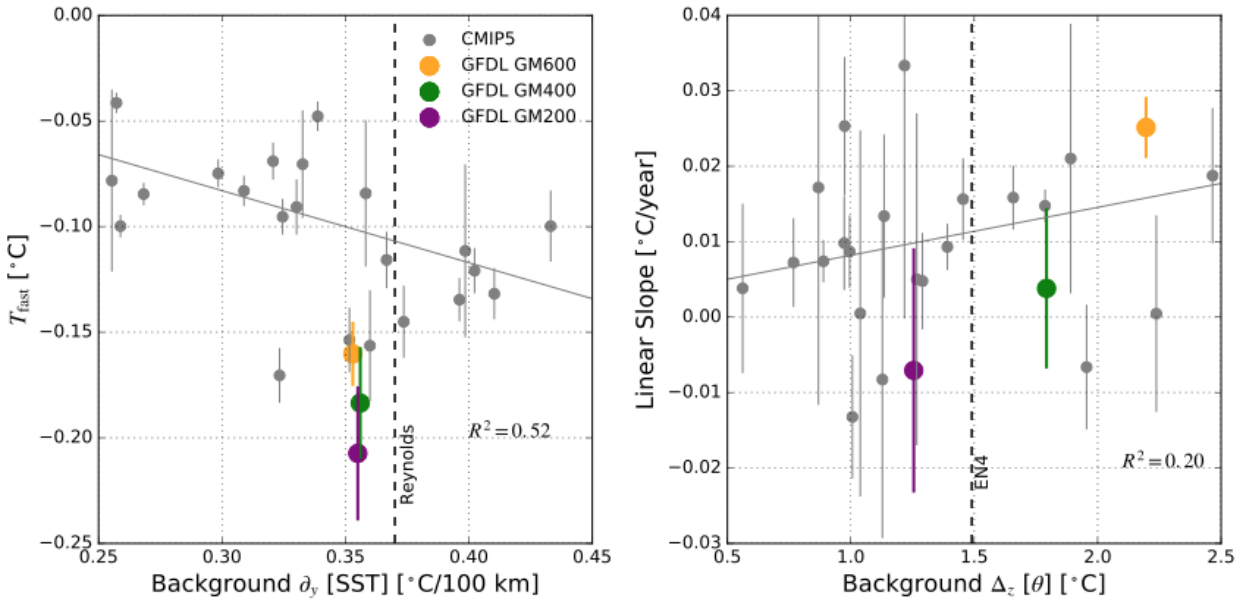

785

786 *Figure 7: Relationship between model climatology and response to a December-May step SAM*
787 *perturbation. (a) Fast (year-1) 50-70°S SST response to the SAM perturbation against the*
788 *climatological (control simulation) meridional SST gradient over 50-70°S. (b) Trend in SST from*
789 *years 1-7 following the SAM perturbation against the climatological annual-mean temperature*
790 *inversion (i.e. maximum vertical temperature contrast) between 67-510 m depth. Error bars*
791 *show ± 1 standard error. The gray line shows the linear fit to the CMIP5 models' scatter, where*
792 *each model has been weighted by the inverse of its standard error squared, the R^2 value for this*
793 *linear regression is shown in each panel. Observational estimates [using data from the NOAA*
794 *Reynolds Optimum Interpolation, Reynolds et al. (2002) and Hadley Centre EN4 dataset, Good*
795 *et al. (2013)] are indicated by the vertical dashed lines.*

796

797

798

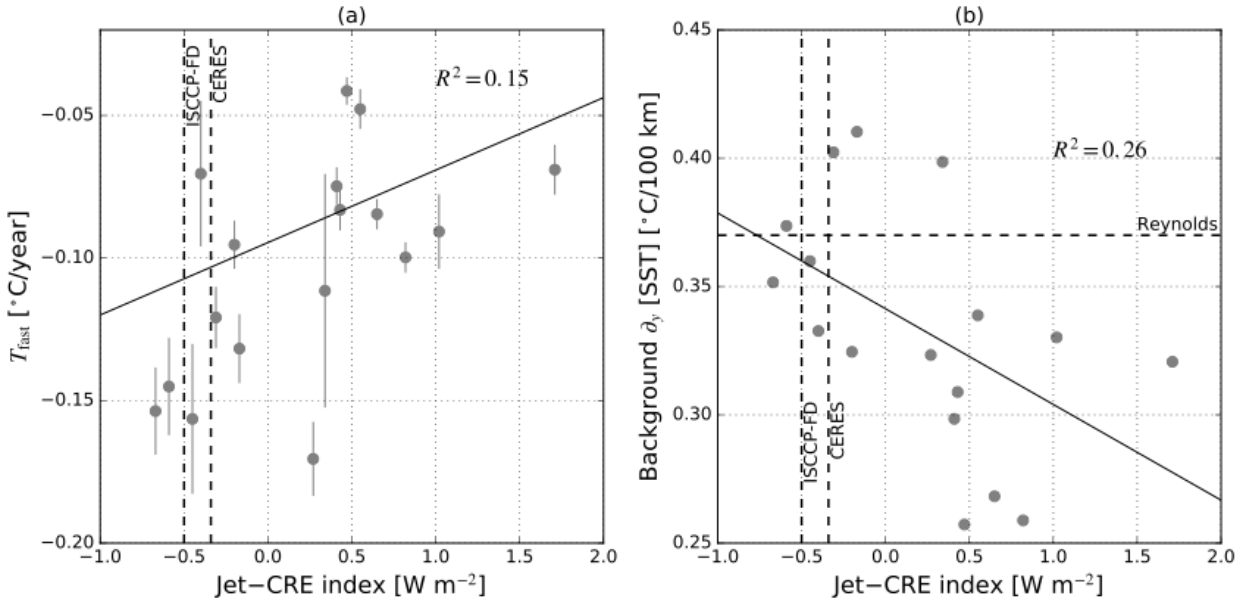

Figure 8: (a) Fast (year-1) 50-70°S SST response to the December-May SAM perturbation (as Fig. 7a) against the December-March jet-CRE index for 17 CMIP5 models reported by Grise and Polvani (2014). (b) Climatological) meridional SST gradient over 50-70°S (as Fig 7a) against the jet-CRE index for the same models. Data for the jet-CRE index are from Grise and Polvani (2014). Correlation coefficients are shown in the upper right of each figure. Two observational estimates of the jet-CRE index from Grise and Polvani (2014) are shown, using either radiative fluxes from the International Satellite Cloud Climatology Project (ISCCP; Zhang et al. 2004) or Clouds and Earth's Radiant Energy System (CERES; Loeb et al. 2012) experiment. As in Fig. 7a, the observational estimate of the meridional SST gradient from Reynolds et al. (2002) is shown by the horizontal line in (b).

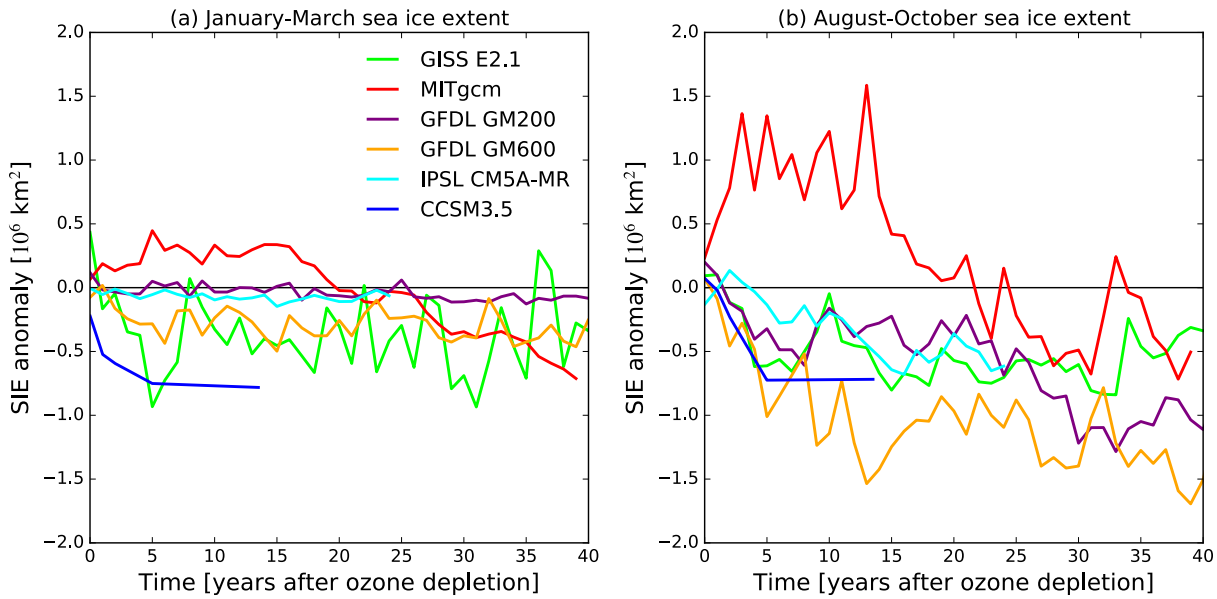

815

816 *Figure 9: Ensemble mean anomalies of January-March (a) and August-October (b) Southern*

817 *Hemisphere sea-ice extent (SIE) in each ozone depletion CRF simulation.*